DEUTSCHES ELEKTRONEN-SYNCHROTRON DESY

DESY 85-045
UAB-FT-122
March 1985

SINGLE WINO PRODUCTION IN e^+e^- COLLISIONS

by

M. Martinez

Deutsches Elektronen-Synchrotron DESY, Hamburg

J.A. Grifols, R. Pascual

Dept. de Física Téorica, Univ. Autónoma de Barcelona, Bellaterra

ISSN 0418-9833

NOTKESTRASSE 85 · 2 HAMBURG 52

DESY 85-045
UAB-FT-122
March 1985

ISSN 0418-9833

SINGLE WINO PRODUCTION IN e^+e^- COLLISIONS

M. Martinez*

Deutsches Elektronen Synchrotron, DESY, Hamburg

J.A. Grifols and R. Pascual

Departament de Física Teòrica

Universitat Autònoma de Barcelona

BELLATERRA (Barcelona), SPAIN

ABSTRACT: We present a detailed analysis of single wino production in e^+e^- collisions. We give total and differential cross sections at three different energies, relevant to present (DESY) and future (LEP) experiments for different choices of sparticle masses. We comment on different approximations (useful at different energy regimes) and discuss on signatures and backgrounds.

---

*.- MARK-J Collaboration (On leave of absence from "Laboratori de Física d'Altes Energies", BELLATERRA (Barcelona), Spain.

1.- INTRODUCTION

Physics at the Fermi scale and below is essentially understood. The standard model provides a theoretical framework that enables one to correlate a large amount of experimental data in a simple and very elegant way. Despite this success the theory as it stands is far from being complete. In fact there is a general belief among physicists that a threshold for new physics must be reached at about the 1 TeV energy scale. The trouble really resides in the scalar sector of the theory which is poorly understood and yet is a fundamental ingredient in the construction of modern spontaneously broken gauge theories. Indeed, Higgs particles must either be found with masses smaller than 1 TeV or else the weak interactions at very high energies ($\gtrsim$ 1 TeV) will be very different from the naïve predictions of the standard SU(2)xU(1) model. A possible scenario which has been recently contemplated as a source of new physics are composite models[1] which give up elementarity of quarks and leptons and/or gauge bosons. The main alternative direction is supersymmetry[2] where one sticks to the gauge dogma and exploits at maximum a new Fermi-Bose symmetry not yet fully explored in realistic quantum field theories.

The quest for phenomenological applications of supersymmetries has led to the formulation of fairly realistic N=1 SUGRA models[3]. The common feature of all these models is the prediction of a supersymmetric particle mass spectrum pretty close to the presently available energies. Many processes have been proposed, both in e^+e^- and in $p\bar{p}$ colliders, as a means for discovering supersymmetry[2]. There are presently some claims that monojet events seen at the CERN $Sp\bar{p}S$ constitute the first positive

signal of supersymmetry[4]. Whatever the final output of this experimental evidence might be, it is fruitful to look closer into the phenomenological consequences of SUSY.

An important task associated to experimental searches for supersymmetry is to set bounds to sparticle masses as a result of non observation of SUSY signals. From e^+e^- annihilation experiments we know already that roughly $\tilde{m} \gtrsim 20$ GeV for squarks and sleptons as well as for charged gauge fermions since their pair production has not been observed. It is clear that one may improve the bound in any of these particle masses if they are singly produced along with a lighter SUSY particle. The aim of the present work is to perform a thorough analysis of single wino production in association with a scalar neutrino in e^+e^- collisions as- suming $M_{\tilde{W}} \gtrsim E_{beam}$. This process has been considered before by Eilam and Reya[5] and by Salati and Wallet[6]. Both these papers work within not fully tested approximations which probably are not reliable at high energies. Here we shall be complete as far as diagrams and cross section calculations is concerned. We shall however use the supergravity model as stated in Ref. (7). This should not be a serious restriction to the general validity of our results.

The plan of the paper is the following. In section 2 we state the amplitudes. Section 3 is devoted to a discussion of the validity of several approximation and of the total and differential cross sections calculated in three different energy regimes: the maximum PETRA energy, the energy around the Z°-pole (LEP) and $\sqrt{s} \simeq 165$ GeV (well beyond the Z° pole). We include also in this section a brief discussion on signatures and backgrounds. In an appendix we collect the results of the squared amplitudes which were obtained using the REDUCE program.

2.- AMPLITUDES FOR $e^+e^- \to e^+\tilde{W}^-\tilde{\nu}$

Besides the two amplitudes which contribute to our process

$$e^+(p_1)+e^-(p_2) \to e^+(p_3)+\tilde{W}^-(p_4)+\tilde{\nu}(p_5)$$

in the (almost real photon) Weiszäcker Williams approximation (diagrams (a) and (b) in Fig. 1) we must consider the diagrams (c)-(f) in Fig. 1, namely two diagrams with s-channel photon and two with t-channel $\tilde{\nu}$ and $\tilde{W}$. Furthermore one must also include diagrams with Z° propagators, mainly if one is interested in energies near or above the Z° pole; in Fig. 2 we show these diagrams. It is clear that to compute the cross section one must go beyond the W.W. approximation since this method cannot be reliable, for example, if the $\tilde{\nu}$ mass is small, in which case diagram (e) of Fig. 1 can be important, or for energies above the Z mass.

The corresponding amplitudes of these twelve diagrams are given, in a self-explanatory notation , by the following expressions:

$$A_{1a} = \frac{i e^3}{\sin\theta_W} \cdot \frac{[\bar{e}^+(p_1)\gamma^\mu e^+(p_3)][\bar{\tilde{W}}^-(p_4)P_L(\not{p}_4+\not{p}_5+M_e)\gamma_\mu e^-(p_2)]}{[(p_1-p_3)^2][(p_4+p_5)^2-M_e^2]}$$

$$A_{1b} = \frac{i e^3}{\sin\theta_W} \cdot \frac{[\bar{e}^+(p_1)\gamma^\mu e^+(p_3)][\bar{\tilde{W}}^-(p_4)\gamma_\mu(\not{p}_2-\not{p}_5+M_{\tilde{W}})P_L e^-(p_2)]}{[(p_1-p_3)^2][(p_2-p_5)^2-M_{\tilde{W}}^2]}$$

$$A_{1c} = \frac{-i e^3}{\sin\theta_W} \cdot \frac{[\bar{e}^+(p_1)\gamma^\mu e^-(p_2)]\cdot[\bar{\tilde{W}}^-(p_4)P_L(\not{p}_4+\not{p}_5+M_e)\gamma_\mu e^+(p_3)]}{[(p_1+p_2)^2]\cdot[(p_4+p_5)^2-M_e^2]}$$

$$A_{1d} = \frac{-ie^3}{\sin\theta_W} \cdot \frac{[\bar{e}^+(p_1)\gamma^\mu e^-(p_2)]\cdot[\bar{\tilde{W}}^-(p_4)\gamma_\mu(-\not{p}_3-\not{p}_5+M_{\tilde{W}})P_L e^+(p_3)]}{[(p_1+p_2)^2]\cdot[(p_3+p_5)^2-M_{\tilde{W}}^2]}$$

$$A_{1e} = \frac{-ie^3}{\sin^3\theta_W} \cdot \frac{[\bar{e}^+(p_1)(-\not{p}_3-\not{p}_5)P_L e^+(p_3)]\cdot[\bar{\tilde{W}}^-(p_4)P_L e^-(p_2)]}{[(p_2-p_4)^2-M_{\tilde{\nu}}^2]\cdot[(p_3+p_5)^2-M_{\tilde{W}}^2]}$$

$$A_{1f} = \frac{ie^3}{\sin^3\theta_W} \cdot \frac{[\bar{e}^+(p_1)(\not{p}_2-\not{p}_5)P_L e^-(p_2)]\cdot[\bar{\tilde{W}}^-(p_4)P_L e^+(p_3)]}{[(p_2-p_5)^2-M_{\tilde{W}}^2][(p_3+p_4)^2-M_{\tilde{\nu}}^2]}$$

$$A_{2a} = ie^2 g\alpha \frac{[\bar{e}^+(p_1)\gamma^\nu(\alpha P_L+\beta P_R)e^+(p_3)][g_{\mu\nu}-k_\mu k_\nu/M_Z^2][\bar{\tilde{W}}^-(p_4)(\not{p}_4+\not{p}_5)\gamma^\mu P_L e^-(p_2)]}{[(p_4+p_5)^2][k^2-M_Z^2+iM_Z\Gamma_Z]}$$

$$A_{2b} = -ie^2 g\cot\theta_W \frac{[\bar{e}^+(p_1)\gamma^\nu(\alpha P_L+\beta P_R)e^+(p_3)][g_{\mu\nu}-k_\mu k_\nu/M_Z^2][\bar{\tilde{W}}^-(p_4)\gamma^\mu(\not{p}_2-\not{p}_5+M_{\tilde{W}})P_L e^-(p_2)]}{[(p_2-p_5)^2-M_{\tilde{W}}^2][k^2-M_Z^2+iM_Z\Gamma_Z]}$$

$$A_{2c} = -ie^2 g\alpha \frac{[\bar{e}^+(p_1)\gamma^\nu(\alpha P_L+\beta P_R)e^-(p_2)][g_{\mu\nu}-Q_\mu Q_\nu/M_Z^2][\bar{\tilde{W}}^-(p_4)(\not{p}_4+\not{p}_5)\gamma^\mu P_L e^+(p_3)]}{[(p_4+p_5)^2][Q^2-M_Z^2+iM_Z\Gamma_Z]}$$

$$A_{2d} = ie^2 g\cot\theta_W \frac{[\bar{e}^+(p_1)\gamma^\nu(\alpha P_L+\beta P_R)e^-(p_2)][g_{\mu\nu}-Q_\mu Q_\nu/M_Z^2][\bar{\tilde{W}}^-(p_4)\gamma^\mu(-\not{p}_3-\not{p}_5+M_{\tilde{W}})P_L e^+(p_3)]}{[(p_3+p_5)^2-M_{\tilde{W}}^2][Q^2-M_Z^2+iM_Z\Gamma_Z]}$$

$$A_{2e} = +ie^2 g\Omega \cdot \frac{[\bar{e}^+(p_1)\gamma^\nu(\alpha P_L+\beta P_R)e^+(p_3)][g_{\mu\nu}-k_\mu k_\nu/M_Z^2][\bar{\tilde{W}}^-(p_4)(p_5+p_2-p_4)^\mu P_L e^-(p_2)]}{[(p_2-p_4)^2-M_{\tilde{\nu}}^2][k^2-M_Z^2+iM_Z\Gamma_Z]}$$

$$A_{2f} = -ie^2 g\Omega \cdot \frac{[\bar{e}^+(p_1)\gamma^\nu(\alpha P_L+\beta P_R)e^-(p_2)][g_{\mu\nu}-Q_\mu Q_\nu/M_Z^2][\bar{\tilde{W}}^-(p_4)(p_5-p_3-p_4)^\mu P_L e^+(p_3)]}{[(p_3+p_4)^2-M_{\tilde{\nu}}^2][Q^2-M_Z^2+iM_Z\Gamma_Z]}$$

where

$$k \equiv p_1 - p_3 \qquad Q \equiv p_1 + p_2 \qquad P_{R,L} \equiv \tfrac{1}{2}(1 \pm \gamma_5)$$

$$\alpha \equiv \frac{2\sin^2\theta_W - 1}{2\sin\theta_W\cos\theta_W} \qquad \beta \equiv \mathrm{tg}\,\theta_W \qquad \Omega \equiv \frac{1}{2\sin\theta_W\cos\theta_W}$$

$$g = e/\sin\theta_W$$

If we denote by A_i each of these twelve amplitudes, and use $A(i,j)=2(\mathrm{Re}\,\{\mathrm{Tr}(A_i \cdot A_j^*)\}$, $A(i,i)=\mathrm{Tr}(A_i \cdot A_i^*)$, the square of the matrix element can be writen

$$|M|^2 = \sum_{j=1}^{12} \sum_{i \le j} A(i,j) \cdot PR(i) \cdot PR(j)$$

where PR(i) denote the corresponding propagators. In the Appendix we present the expression of the matrix element for two special approximations appropriate for DESY and LEP energies.

3. RESULTS

We have computed total and differential cross section for our process at $\sqrt{s}$ equal to 45, 93 and 165 GeV. In each case we have chosen several values of the SUSY particle masses. In order to integrate the sharp peak in the differential cross section due to the contribution of the t-channel photon diagrams (1a,1b) we have used the adaptative multi-dimensional integration algorithm VEGAS[8] with surprisingly good results. In Fig. 3 we plot the total cross section obtained with our complete amplitude for $\sqrt{s}$=45 and $M_{\tilde{\gamma}}$=0 versus $M_{\tilde{W}}$ and compare it with the cross section obtained with the W.W. approximation. As expected, we

notice that the W.W. approximation is reliable only for $M_{\tilde{W}}$ much larger than the beam energy E_b, since otherwise other diagrams become important. The situation is still worse at higher energies where the Z exchanges become dominant.

Furthermore, the kinematics that makes the W.W. approximation reliable, requires the final positron (in $e^+e^- \to e^+\tilde{W}^-\tilde{\nu}$) to be lost inside the beam pipe so that only one charged particle would be detected. In order to exploit the existing luminosity obtained with two charged particles triggers, it is important to know which part of the total cross section comes from events in which one positron is lost in the beam pipe. To answer this question we show in Fig. 4 a sample of the cross section integrated over all positron production angle θ_e (curve a) and introducing a cut of 5° ($|\cos\theta_e| > 0.996$) (curve b) which is the usual experimental condition for most detectors. We notice that in both cases the cross sections are of the same order, showing that one can exploit the two electrically charged particle luminosity to give bounds on the $\tilde{W}$ mass.

We have checked that there are subsets of the twelve diagrams which can be used to estimate the cross sections with good approximation at certain energies. The six diagrams of Fig. 1 for $\sqrt{s}$=45 GeV give cross sections which are only 6% smaller than the exact values. At $\sqrt{s}$=93 the subset of diagrams a, b, e of Fig. 1 and c, d, f of Fig. 2 gives the cross sections with an error smaller than 1%. Notice also that this same subset of diagrams for $\sqrt{s}$=45 GeV overestimates the cross sections by 20%.

In Fig. 5 we plot the cross sections for $\sqrt{s}$ equal to 45 and 93 GeV for different values of $\tilde{\nu}$ and $\tilde{W}$ masses. The values of the cross section for $\sqrt{s}$=165 GeV are given in Table 1. In Fig. 6 we show the differen-

tial cross sections $d\sigma/d(\cos\theta_{\tilde{W}})$ and $d\sigma/dE_{\tilde{W}}$ for $\sqrt{s}$=45 and 93 GeV. We observe that the angular distribution of $\tilde{W}$ is almost flat and that the $\tilde{W}$ is produced mainly at rest. So the electrons coming from the eventual decay of $\tilde{W}^- \to e^-\tilde{\nu}$ will be isotropically distributed, i.e., uncorrelated with the directly produced positron. In Fig. 7 we plot $d\sigma/d(\cos\theta_e)$ and $d\sigma/dE_e$. Notice that $d\sigma/d(\cos\theta_e)$ presents a forward peak which becomes less pronounced at higher energies (where the W.W. approximation is less reliable).

Finally let us shortly comment on signatures and backgrounds. We shall assume that the $\tilde{W}^-$ decays mainly into $\ell^-\tilde{\nu}$ and that the scalar neutrino escapes detection. There are therefore two charged leptons in the final state. The lepton coming from $\tilde{W}$ decay carries an energy larger or about one half the wino mass; the other one is slower and very forward as seen from Fig.7. These facts suggest the following signatures: the detection of a "single lepton" with $E_\ell \gtrsim M_{\tilde{W}}/2$ and/or "double lepton" detection with both leptons very acoplanar and with very different energies ($E_\ell \gtrsim M_{\tilde{W}}/2$ for the first and $E_\ell \ll E_b$ for the second). These very distinct characteristics make it easy to identify the events as having a SUSY origin and make it rather difficult to confuse them with ordinary QED background: $l\bar{l}\gamma$ production with $l\gamma$ not detected in the "single lepton" case or with γ not detected in the "double lepton" case and (one order of α higher) $l\bar{l}l'\bar{l}'$ production with three or two not detected leptons in the "single" and "double lepton" cases respectively.

APPENDIX

In order to compute the $e^+e^- \to e^+\bar{W}^-\bar{\nu}$ cross section we can use a subset of the twelve diagrams which contribute to the exact cross sec- tion. One subset is appropriate for energies much below the Z° pole (DESY) and the other one can be used for energies near or beyond the Z°. We show here the output of the REDUCE computation of these subsets.

A) PETRA Energies (diagrams (1a,1b,1c,1d,1e and 1f))

Defining

$$p_{ij} \equiv p_i \cdot p_j$$

$$(p_i, s_1, s_2, s_3) \equiv p_{1i}(s_1 p_{3i} p_{12} + s_2 p_{2i} p_{13} + s_3 p_{1i} p_{23})$$

$$(s_1, s_2, s_3) \equiv p_{15}(s_1 p_{45} p_{23} + s_2 p_{35} p_{24} + s_3 p_{34} p_{25})$$

for $S_k = +,0,-$ $(k=1,2,3)$ we have for the squared matrix elements:

$$A(1a,1a) = 16C_1\{M_W^2(p_{12}(2p_{35}+p_{34}) + p_{23}(2p_{15}+p_{14})) - M_W^2(p_{34}p_{12} + p_{23}p_{14}) + 2p_{45}(p_{35}p_{12} + p_{23}p_{15})\}$$

$$A(1b,1b) = 16C_1\{M_W^2(p_{34}p_{12} + 2p_{35}p_{13} + p_{23}p_{14}) - M_W^2(p_{34}p_{12} + p_{23}p_{14}) + 2p_{25}(p_{35}p_{14} + p_{34}p_{15})\}$$

$$A(1c,1c) = A(1a,1a;\ p_2 \leftrightarrow -p_3)$$

$$A(1d,1d) = A(1b,1b;\ p_2 \leftrightarrow -p_3)$$

$$A(1e,1e) = -4C_2\{M_W^2 p_{34}p_{13} - 2p_{35}p_{24}p_{15}\}$$

$$A(1f,1f) = A(1e,1e;\ p_2 \leftrightarrow -p_3)$$

$$A(1a,1b) = 32C_1\{M_W^2(p_{12}(p_{35}+p_{34}) + p_{23}(p_{15}+p_{14}) + p_{23}p_{13}) + (p_5 - + -) + p_{45}(p_{35}p_{12} + p_{23}p_{15}) + p_{35}(p_{25}p_{14} - 2p_{34}p_{15}) + p_{34}p_{25}p_{15}\}$$

$$A(1a,1c) = 32C_1\{M_W^2 p_{23}(-2p_{15} - p_{14}) + M_W^2 p_{23}p_{14} - 2p_{45}p_{23}p_{15}\}$$

$$A(1a,1d) = 16C_1\{M_W^2(-p_{35}p_{12} + p_{25}p_{13} - p_{23}(3p_{15}+2p_{14})) + (p_5 - + +) + 2(- - +)\}$$

$$A(1a,1e) = 8C_3\{(p_4 - + -) + (p_5 - + +) + 2(- - +)\}$$

$$A(1a,1f) = 8C_3\{(p_4 - + +) + (p_5 - + -) + 2(- - +)\}$$

$$A(1b,1c) = 16C_1\{M_W^2(p_{35}p_{12} - p_{25}p_{13} - p_{23}(3p_{15}+2p_{14})) + (p_5 + - +) + 2(- + -)\}$$

$$A(1b,1d) = 16C_1\{-2M_W^2 p_{23}(p_{14}+p_{15}) + (p_5 - - +) + 2(- + +)\}$$

$$A(1b,1e) = 8C_3\{(p_4 - + -) + (p_5 - - +) + 2(- + +)\}$$

$$A(1b,1f) = 8C_3\{(p_4 - + +) - 2M_W^2 p_{34}p_{12} + 4(0\,0\,+)\}$$

$$A(1c,1d) = 32C_1\{M_W^2(p_{35}p_{12} + p_{12}(p_{25}+p_{24}) + p_{23}(p_{15}+p_{14})) + (p_5 + - -) + p_{45}(p_{25}p_{12} + p_{23}p_{15}) + p_{35}(p_{25}p_{14} + p_{24}p_{15}) - 2p_{34}p_{25}p_{15}\}$$

$$A(1c,1e) = 8C_3\{(p_4 + - +) + (p_5 + - -) + 2(+ + -)\}$$

$$A(1c,1f) = 8C_3\{(p_4 + - -) + (p_5 + - +) + 2(- + -)\}$$

$$A(1d,1e) = 8C_3\{(p_4 + - +) - 2M_W^2 p_{24}p_{13} + 4(0\,+\,0)\}$$

$$A(1d,1f) = 8C_3\{(p_4 + - -) + (p_5 - - +) + 2(- + +)\}$$

$$A(1e,1f) = 4C_2\{(p_5 - - +) + 2(- + +)\}$$

where, we have used the following definitions

$$K_1 \equiv (e)^{3/2}/\sin\theta_W$$

$$K_2 \equiv K_1/\sin^2\theta_W$$

$$C_1 \equiv K_1^2 \qquad C_2 \equiv K_2^2 \qquad C_3 \equiv K_1 K_2$$

Notice that propagators are defined including the global sign in front of the "i" of each amplitude: that means, that they include, the global sign of the diagram.

B) LEP Energies (diagrams (1a,1b,1e,2c,2d and 2f))

Defining now,

$$(L, s_1, s_2, s_3, s_4) \equiv M_W^2 \left(s_1 p_{35} p_{12} + s_2 p_{45} p_{13} + s_3 p_{23} p_{15} + s_4 p_{23} p_{14}\right)$$

$$(R, s_1, s_2, s_3, s_4) \equiv M_W^2 \left(s_1 p_{35} p_{12} + s_2 p_{45} p_{13} + s_3 p_{24} p_{13} + s_4 p_{23} p_{15}\right)$$

$$(L, s_1, s_2, s_3) \equiv s_1 p_{45} p_{23} p_{15} + s_2 p_{35} p_{24} p_{15} + s_3 p_{34} p_{25} p_{15}$$

$$(R, s_1, s_2, s_3) \equiv s_1 p_{45} p_{23} p_{13} + s_2 p_{35} p_{25} p_{14} + s_3 p_{34} p_{25} p_{15}$$

for s_k=-,0,+,2,3 (k=1,2,3,4) we have

$$A(2c,2c) = -16\, C_{2c}^2 \left\{\alpha^2\left((p_5 00+) - (L\,00\,2+) + 2(L-00)\right) + \beta^2\left((p_5 0+0) - (R\,02+0) + 2(R-00)\right)\right\}$$

$$A(2d,2d) = -16\, C_{2d}^2 \left\{\alpha^2\left((p_5 0+0) + (L-+--) + 2(L\,0-0)\right) + \beta^2\left((p_5 00+) + (R---+) + 2(R\,0-0)\right)\right\}$$

$$A(2f,2f) = -16\, C_{2f}^2 \left\{(\alpha^2+\beta^2)\, p_{34}\left(M_W^2\, p_{12} - 2\, p_{25}\, p_{15}\right)\right\}$$

$$A(2c,2d) = 16\, C_{2c} C_{2d} \left\{\alpha^2\left((p_5+--) + (L+-32) + 2(L++-)\right) + \beta^2\left((p_5+--) + (R+32-) + 2(R++-)\right)\right\}$$

$$A(2d,2f) = -16\, C_{2d} C_{2f} \left\{\alpha^2\left((p_5+-+) + (L+--0) + 2(L-+-)\right) + \beta^2\left((p_5++-) + (R+-0-) + 2(R-+-)\right)\right\}$$

$$A(2c,2f) = 16\, C_{2c} C_{2f} \left\{\alpha^2\left((p_5++-) + (L-++0) + 2(L+--)\right) + \beta^2\left((p_5+-+) + (R-+0+) + 2(R+--)\right)\right\}$$

$$A(1a,2c) = 32\alpha\, C_{2c} K_1 \left\{p_2\, p_{23}\left(M_W^2\, p_{14} + M_W^2(-p_{14} - 2p_{15}) - 2\, p_{45}\, p_{15}\right)\right\} / SM$$

$$A(1a,2d) = -16\alpha\, C_{2d} K_1 \left\{G_Z + p_Z\left((p_5+--) + (L+-32) + 2(L++-)\right)\right\}/SM$$

$$A(1a,2f) = 16\alpha\, C_{2f} K_1 \left\{G_Z + p_Z\left((p_5+-+) + (L+--0) + 2(L-+-)\right)\right\}/SM$$

$$A(1b,2c) = -16\alpha\, C_{2c} K_1 \left\{G_Z + p_Z\left((p_5-+-) + (L-+32) + 2(L+-+)\right)\right\}/SM$$

$$A(1b,2d) = -16\alpha\, C_{2d} K_1 \left\{G_Z + p_Z\left((p_5++-) + (L\,00\,22) + 2(L+--)\right)\right\}/SM$$

$$A(1b,2f) = 16\alpha\, C_{2f} K_1 \left\{\hat{G}_Z + p_Z\left((p_5\,200) + (L+--0) + 4(L\,00-)\right)\right\}/SM$$

$$A(1e,2c) = -8\alpha\, C_{2c} K_2 \left\{G_Z + p_Z\left((p_5-++) + (L-+-0) + 2(L--+)\right)\right\}/SM$$

$$A(1e,2d) = -8\alpha\, C_{2d} K_2 \left\{\hat{G}_Z + p_Z\left((p_5\,020) + (L-+-0) + 4(L\,0-0)\right)\right\}/SM$$

$$A(1e,2f) = -8\alpha\, C_{2f} K_1 \left\{G_Z - \hat{G}_Z + p_Z\left((p_5--+) + 2(L-++)\right)\right\}/SM$$

where

$$C_{2c} \equiv \alpha K_1 \quad , \quad C_{2d} \equiv K_1/\beta \quad , \quad C_{2f} \equiv K_1/\sin 2\theta_W$$

$$p_Z \equiv (p_1+p_2)^2 - M_Z^2 \quad , \quad \gamma_Z \equiv \Gamma_Z M_Z \quad , \quad SM \equiv (p_Z^2 + \gamma_Z^2)^{1/2}$$

$$G_e \equiv \gamma_Z\, \epsilon_{\mu\rho\nu\sigma}\, p_4^\mu\, p_2^\rho\, p_3^\nu\, p_4^\sigma$$

$$\hat{G}_Z \equiv -M_W^2\, G_e \qquad G_Z \equiv -\left(M_W^2 - M_V^2 + 2p_{15}\right) G_e$$

Here the propagators are again defined including the global sign in front of the "i" of each amplitude. In the Z* propagators, only the modulus must be included (because the phase has been already included in the trace calculation).

ACKNOWLEDGEMENTS

The authors wish to thank the members of the MARK-J collaboration and very specially Prof. Min Chen for their interest and many fruitful discussions and also J. Berdugo, C. Maña and J. Solà for their help in some aspects of this calculation. We wish to thank also Dr. X. Tata who calculated the amplitudes independently and Dr. F. Cornet for his interest. Finally we wish to thank the DESY directorate for their hospitality.

This work was partially supported by research project CAICYT (Spain).

FIGURE CAPTION

Fig. 1.- Diagrams contributing to $e^+e^- \to e^+\tilde{W}^-\tilde{\nu}$ without inclusion of the Z°

Fig. 2.- Diagrams contributing to $e^+e^- \to e^+\tilde{W}^-\tilde{\nu}$ with a Z° propagator.

Fig. 3.- Total cross section for $e^+e^- \to e^\pm\tilde{W}^\mp\tilde{\nu}$ vs $\tilde{W}$ mass, for $M_{\tilde{\nu}}=0$ and $\sqrt{s}=$ 45 GeV. The solid points corresponds to the exact value and the solid squares to the Weizsäcker-Williams approximation.

Fig.4.- Sample of single wino production cross section summing over all $e^\pm$ production angles (curve a) and imposing a cut $|\cos\theta_e|>$ 0.996 (curve b).

Fig. 5.- Total cross section for $e^+e^- \to e^\pm\tilde{W}^\mp\tilde{\nu}$.

Fig. 6.- Differential cross sections for $e^+e^- \to e^+\tilde{W}^-\tilde{\nu}$ vs the $\tilde{W}^-$ production angle and vs the $\tilde{W}^-$ energy.

Fig. 7.- Differential cross sections for $e^+e^- \to e^+\tilde{W}^-\tilde{\nu}$ vs the e^+ production angle and vs the e^+ energy.

TABLE CAPTION

Table I.- Values of the cross section for $e^+e^- \to e^\pm\tilde{W}^\mp\tilde{\nu}$ at $\sqrt{s}$=165 GeV for different choices of $\tilde{W}^-$ and $\tilde{\nu}$ masses.

REFERENCES

(1) For a review see, e.g., H. Fritzsch, MPI-PAE/PTh 41/84 abd R.D. Peccei, MPI-PAE/PTh 42/84 and references therein.

(2) H.P. Nilles, Phys. Rep. 110C, 1 (1984); H.E. Haber and G.L. Kane, Phys. Rep., in press.

(3) L.E. Ibáñez, Proceedings of XIIth Winter Meeting on Fundamental Physics, Santillana del Mar (Spain), april 1984, FTUAM preprint 84/7.

(4) M.J. Herrero, L.E. Ibáñez, C. López and F.J. Ynduráin, preprint FTUAM 84/9 (June 1984); J. Ellis and H. Kowalski, DESY 84-045, May 1984.

(5) G. Eilam and E. Reya, Phys. Lett. 145B, 425 (1984) and 148B, 502 (1984).

(6) P. Salati and J.C. Wallet, Phys. Lett. 122B, 397 (1983).

(7) R. Arnowitt, A.H. Chamsedine and P. Nath, Phys. Rev. Lett. 49, 970 (1982) and 50, 232 (1983).

(8) G.P. Lepage, Journal of Computational Phys. 27, 192 (1978).

σ(pb)	$M_{\tilde{\gamma}} = 0$	$M_{\tilde{\gamma}} = 10$ GeV	$M_{\tilde{\gamma}} = 20$ GeV	$M_{\tilde{\gamma}} = 30$ GeV
$M_{\tilde{W}}$=85 GeV	1.08(1)	.0978(8)	.0756(6)	.0528(4)
$M_{\tilde{W}}$=90 GeV	.0644(4)	.0586(4)	.0460(2)	.0325(1)
$M_{\tilde{W}}$=95 GeV	.0432(2)	.0391(2)	.0304(1)	.02116(6)
$M_{\tilde{W}}$=100 GeV	.0292(2)	.026(1)	.0201(1)	.01356(4)

TABLE 1

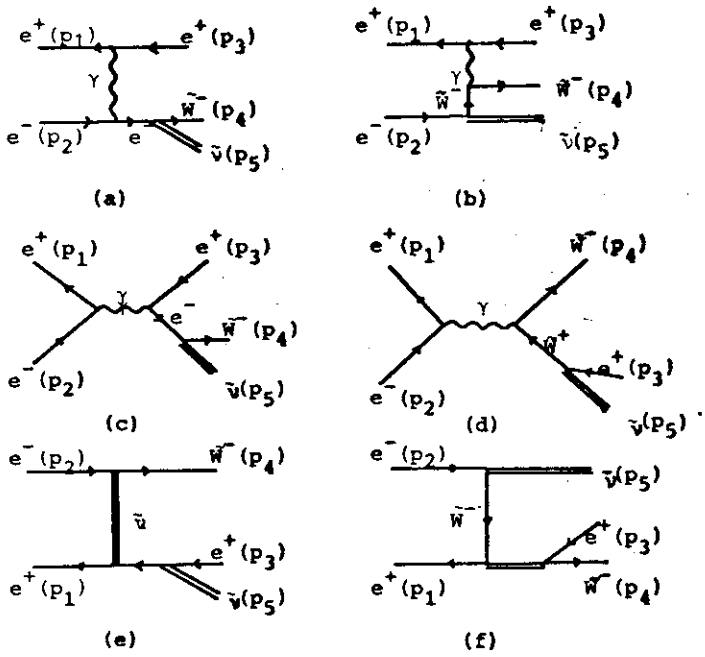

FIG. 1

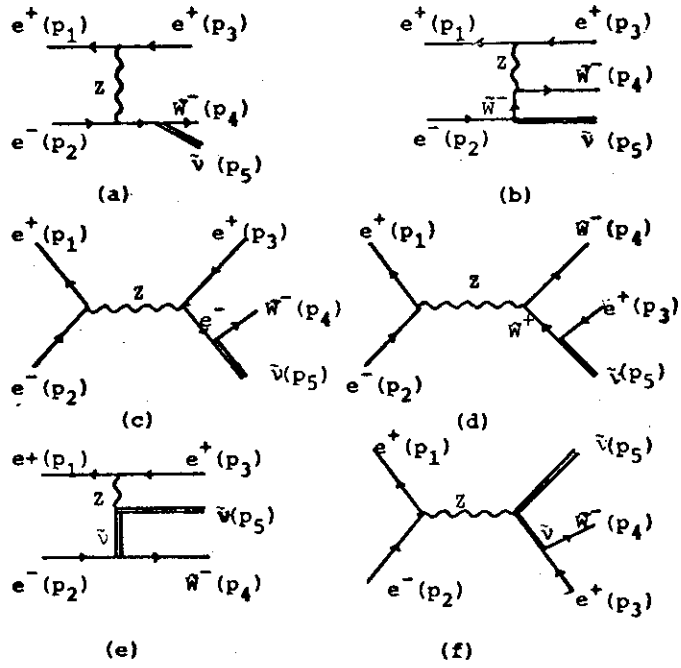

FIG. 2

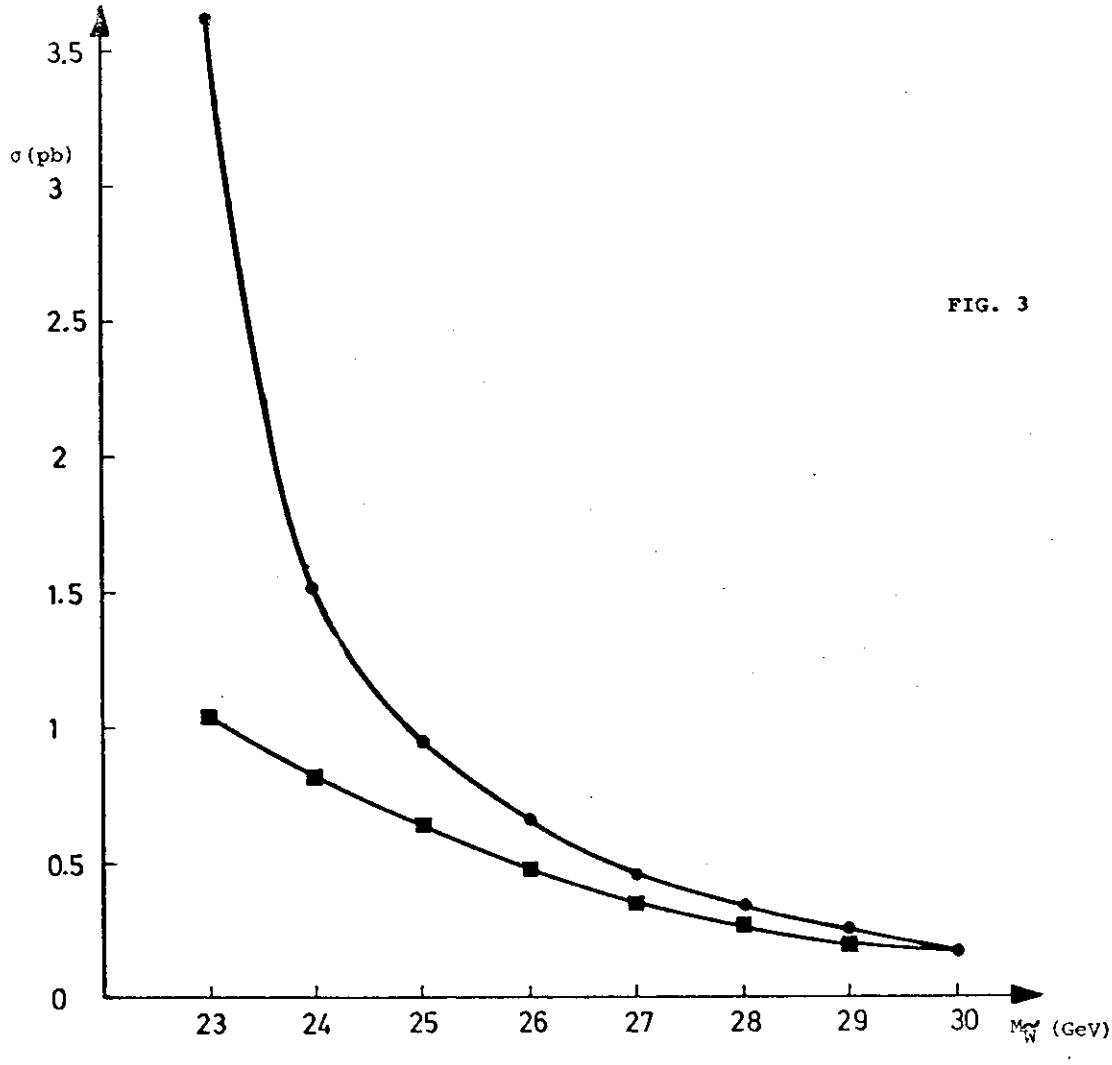

FIG. 3

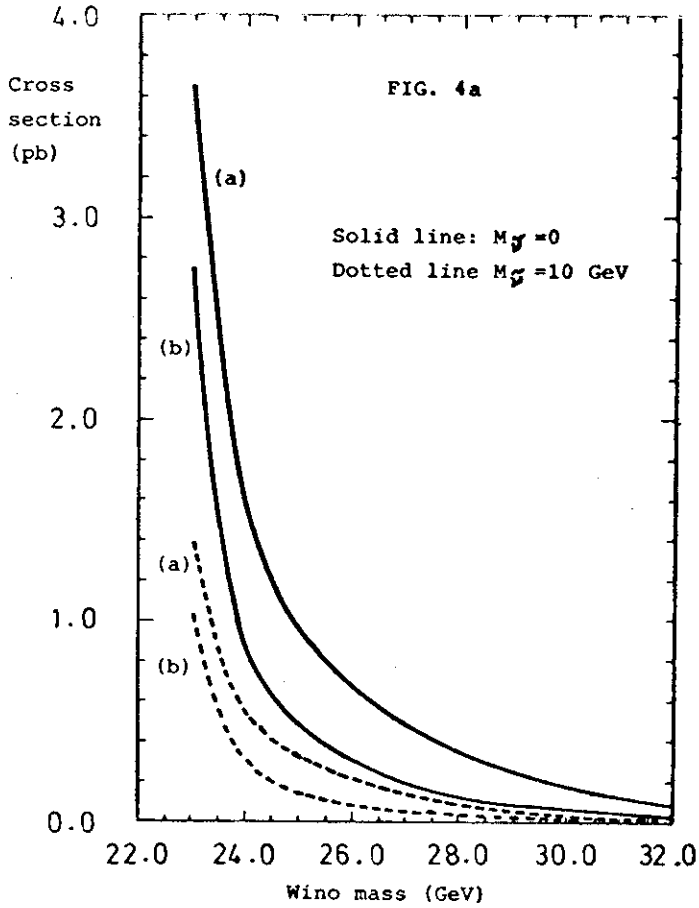
FIG. 4a
Cross section (pb)
4.0
3.0
2.0
1.0
0.0
(a)
(b)
(a)
(b)
Solid line: $M_{\tilde{\nu}}$ =0
Dotted line $M_{\tilde{\nu}}$ =10 GeV
22.0
24.0
26.0
28.0
30.0
32.0
Wino mass (GeV)

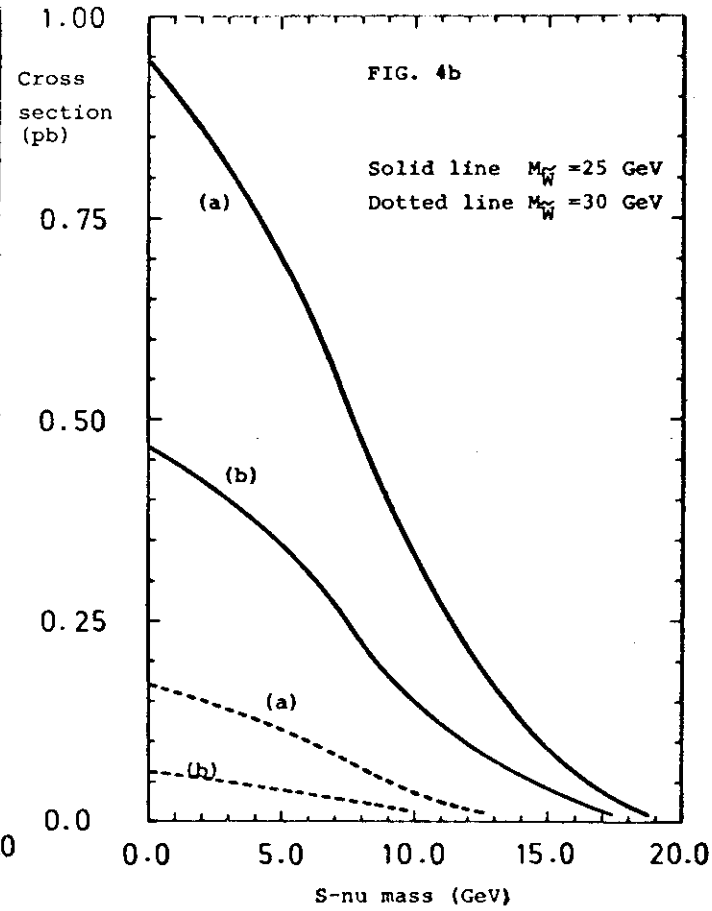
FIG. 4b
Cross section (pb)
1.00
0.75
0.50
0.25
0.0
(a)
(b)
(a)
(b)
Solid line $M_{\tilde{W}}$ =25 GeV
Dotted line $M_{\tilde{W}}$ =30 GeV
0.0
5.0
10.0
15.0
20.0
S-nu mass (GeV)

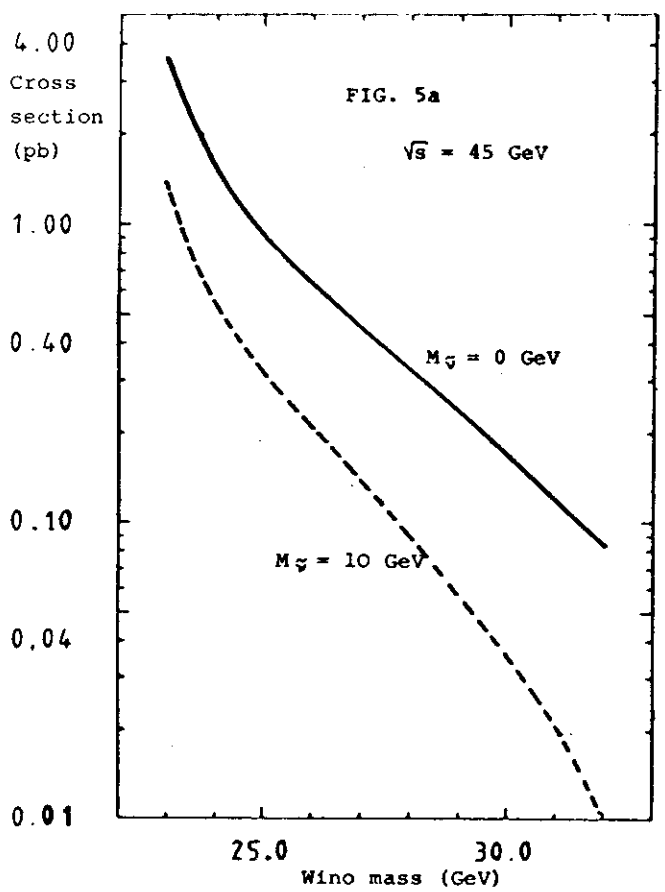
FIG. 5a
Cross section (pb)
4.00
1.00
0.40
0.10
0.04
0.01
$\sqrt{s}$ = 45 GeV
$M_{\tilde{\nu}}$ = 0 GeV
$M_{\tilde{\nu}}$ = 10 GeV
25.0
30.0
Wino mass (GeV)

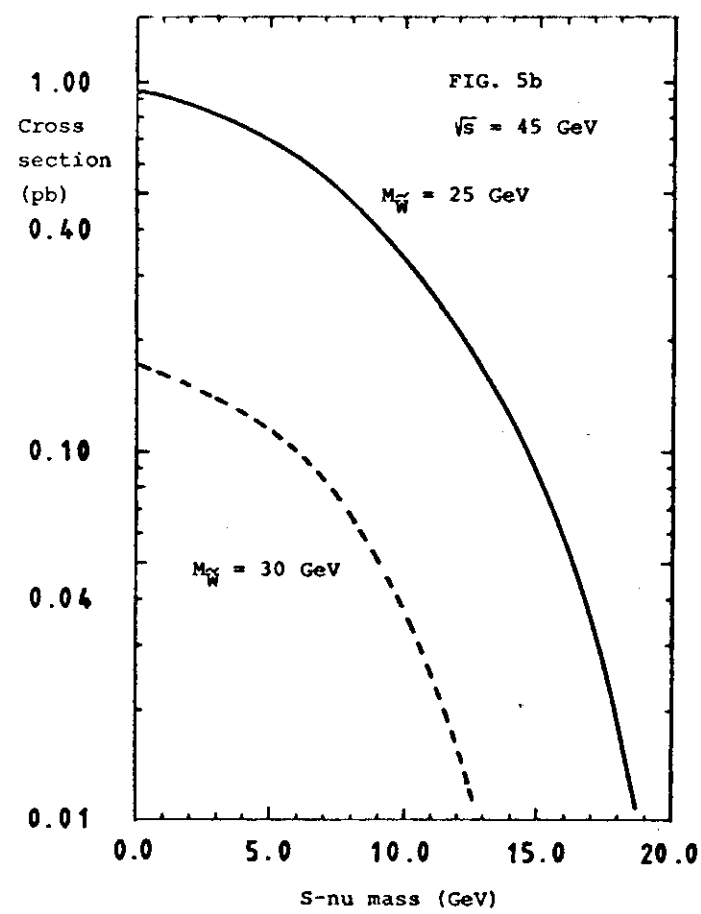
FIG. 5b
Cross section (pb)
1.00
0.40
0.10
0.04
0.01
$\sqrt{s}$ = 45 GeV
$M_{\tilde{W}}$ = 25 GeV
$M_{\tilde{W}}$ = 30 GeV
0.0
5.0
10.0
15.0
20.0
S-nu mass (GeV)

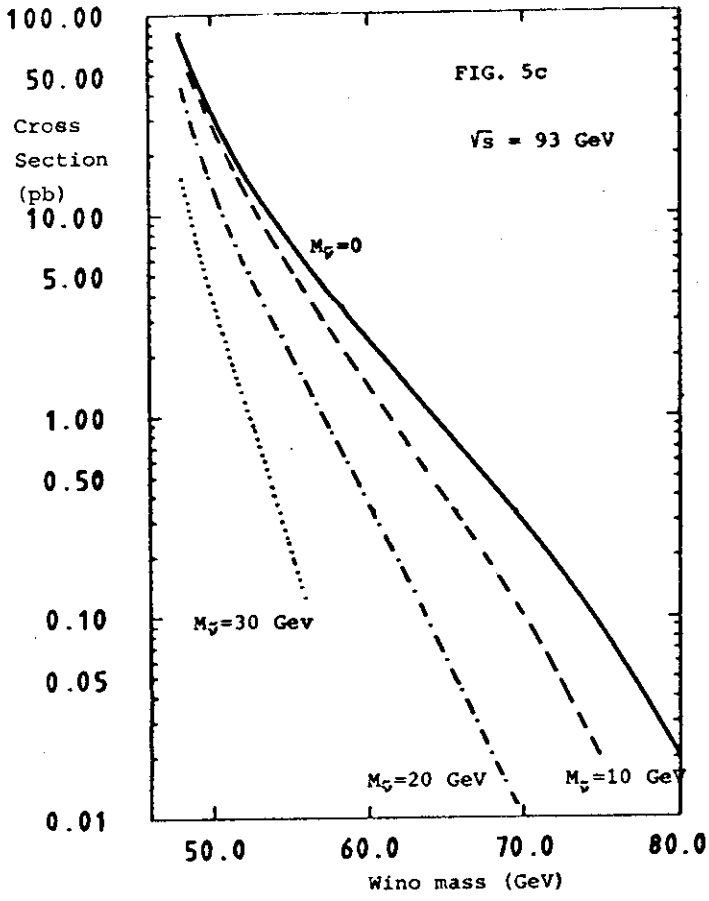
FIG. 5c
$\sqrt{s}$ = 93 GeV
Cross Section (pb)
100.00
50.00
10.00
5.00
1.00
0.50
0.10
0.05
0.01
$M_{\tilde{\nu}}$=0
$M_{\tilde{\nu}}$=30 Gev
$M_{\tilde{\nu}}$=20 GeV
$M_{\tilde{\nu}}$=10 GeV
50.0
60.0
70.0
80.0
Wino mass (GeV)

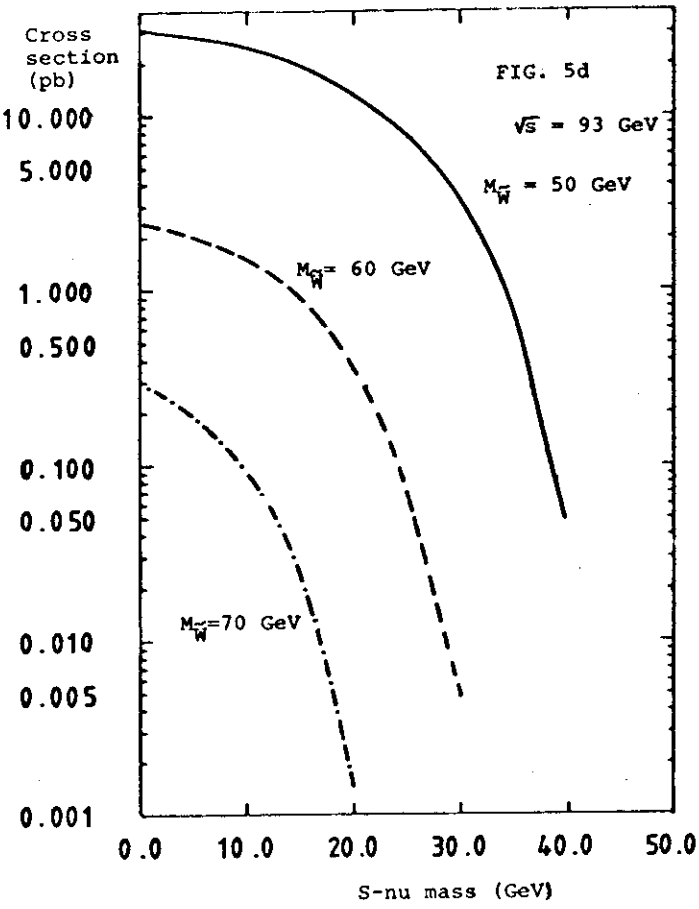
FIG. 5d
$\sqrt{s}$ = 93 GeV
$M_{\tilde{W}}$ = 50 GeV
Cross section (pb)
10.000
5.000
1.000
0.500
0.100
0.050
0.010
0.005
0.001
$M_{\tilde{W}}$= 60 GeV
$M_{\tilde{W}}$=70 GeV
0.0
10.0
20.0
30.0
40.0
50.0
S-nu mass (GeV)

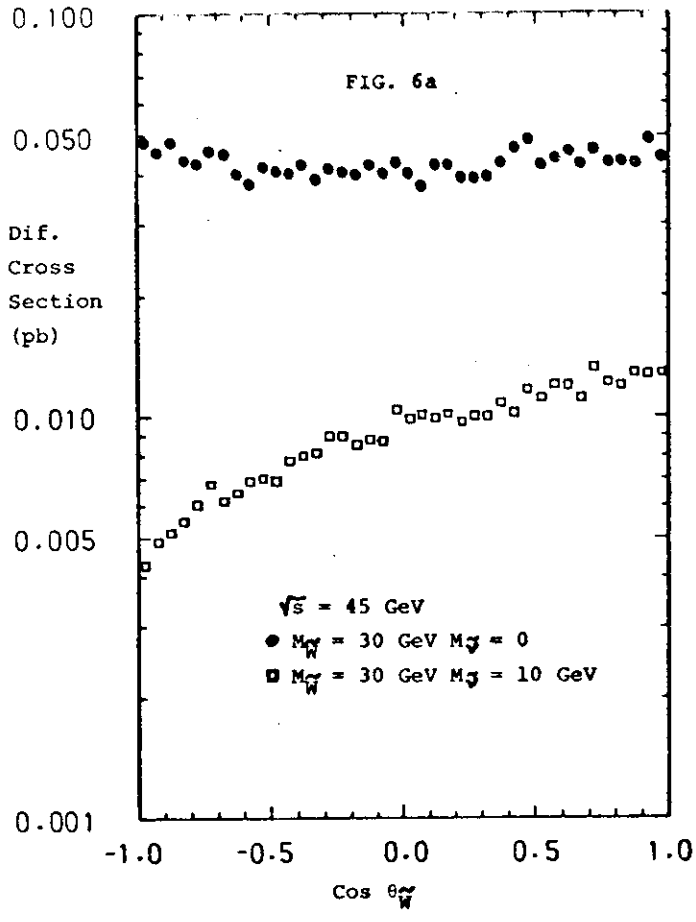
FIG. 6a
Dif. Cross Section (pb)
0.100
0.050
0.010
0.005
0.001
$\sqrt{s}$ = 45 GeV
$M_{\tilde{W}}$ = 30 GeV $M_{\tilde{\nu}}$ = 0
$M_{\tilde{W}}$ = 30 GeV $M_{\tilde{\nu}}$ = 10 GeV
-1.0
-0.5
0.0
0.5
1.0
Cos $\theta_{\tilde{W}}$

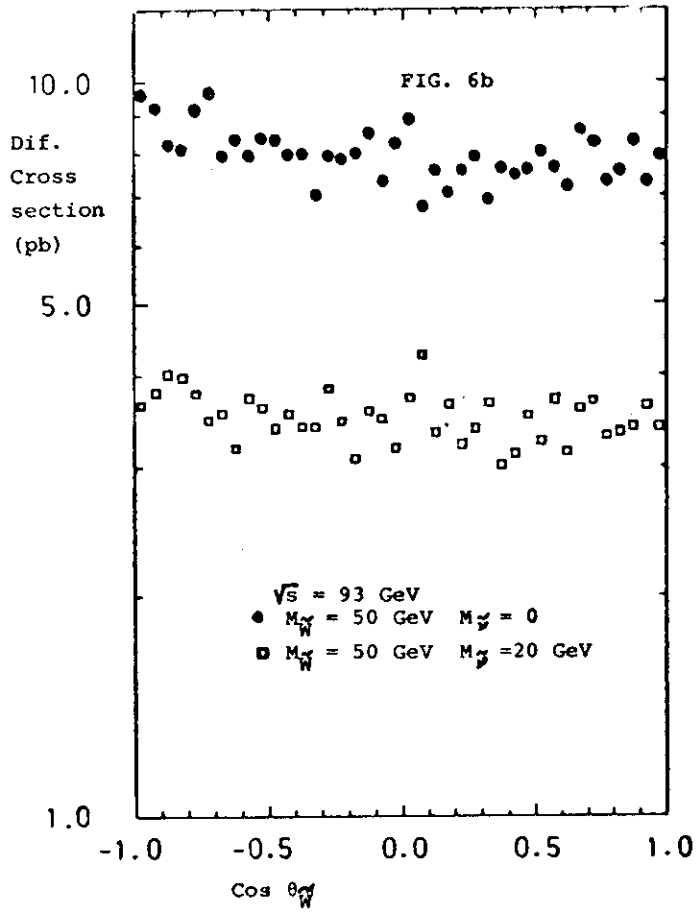
FIG. 6b
Dif. Cross section (pb)
10.0
5.0
1.0
$\sqrt{s}$ = 93 GeV
$M_{\tilde{W}}$ = 50 GeV $M_{\tilde{\nu}}$ = 0
$M_{\tilde{W}}$ = 50 GeV $M_{\tilde{\nu}}$ =20 GeV
-1.0
-0.5
0.0
0.5
1.0
Cos $\theta_{\tilde{W}}$

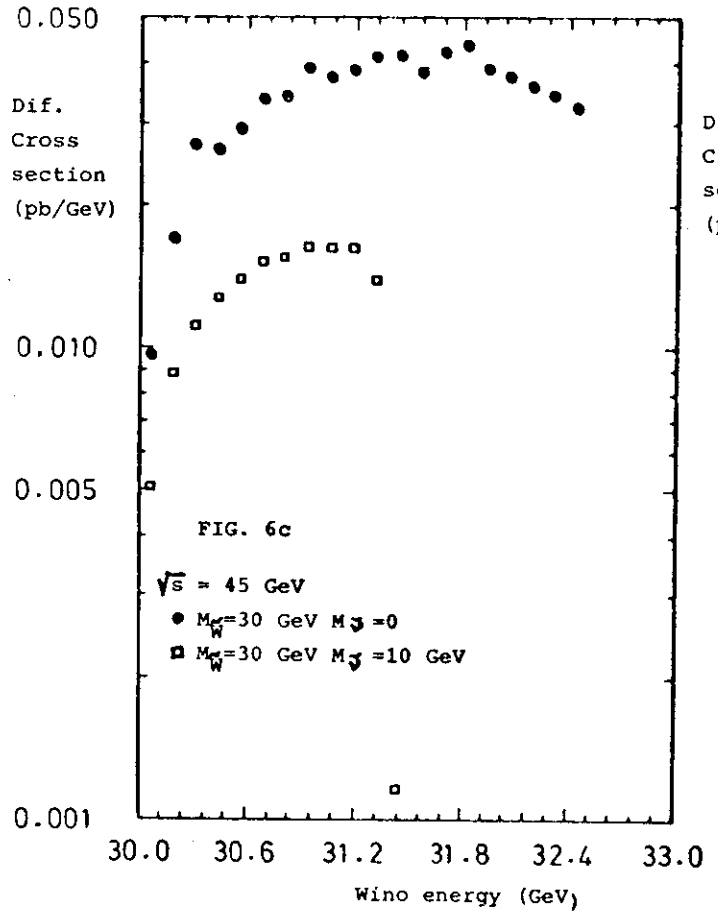
0.050
Dif.
Cross
section
(pb/GeV)
0.010
0.005
0.001
FIG. 6c
√s = 45 GeV
● $M_{\tilde{W}}$=30 GeV $M_{\tilde{\nu}}$=0
□ $M_{\tilde{W}}$=30 GeV $M_{\tilde{\nu}}$=10 GeV
30.0
30.6
31.2
31.8
32.4
33.0
Wino energy (GeV)

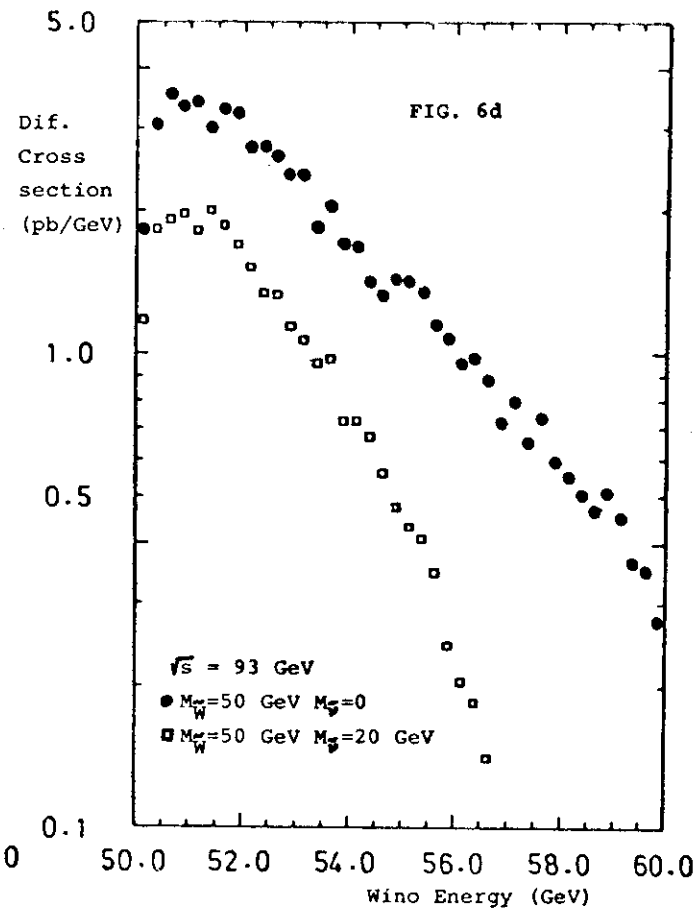
5.0
Dif.
Cross
section
(pb/GeV)
1.0
0.5
0.1
FIG. 6d
√s = 93 GeV
● $M_{\tilde{W}}$=50 GeV $M_{\tilde{\nu}}$=0
□ $M_{\tilde{W}}$=50 GeV $M_{\tilde{\nu}}$=20 GeV
50.0
52.0
54.0
56.0
58.0
60.0
Wino Energy (GeV)

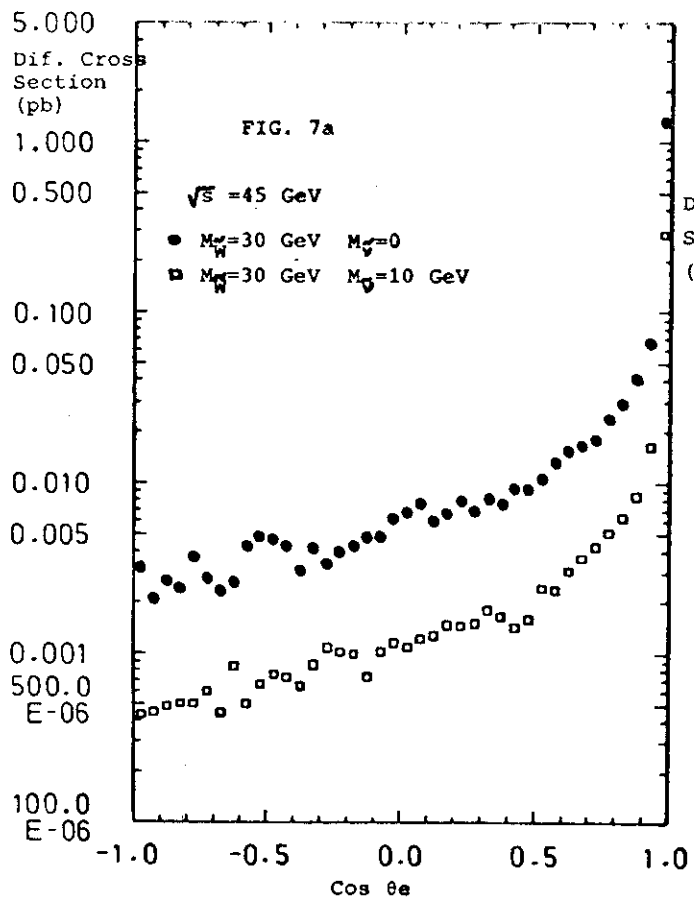
5.000
Dif. Cross
Section
(pb)
1.000
0.500
0.100
0.050
0.010
0.005
0.001
500.0
E-06
100.0
E-06
FIG. 7a
√s =45 GeV
● $M_{\tilde{W}}$=30 GeV $M_{\tilde{\nu}}$=0
□ $M_{\tilde{W}}$=30 GeV $M_{\tilde{\nu}}$=10 GeV
-1.0
-0.5
0.0
0.5
1.0
Cos θe

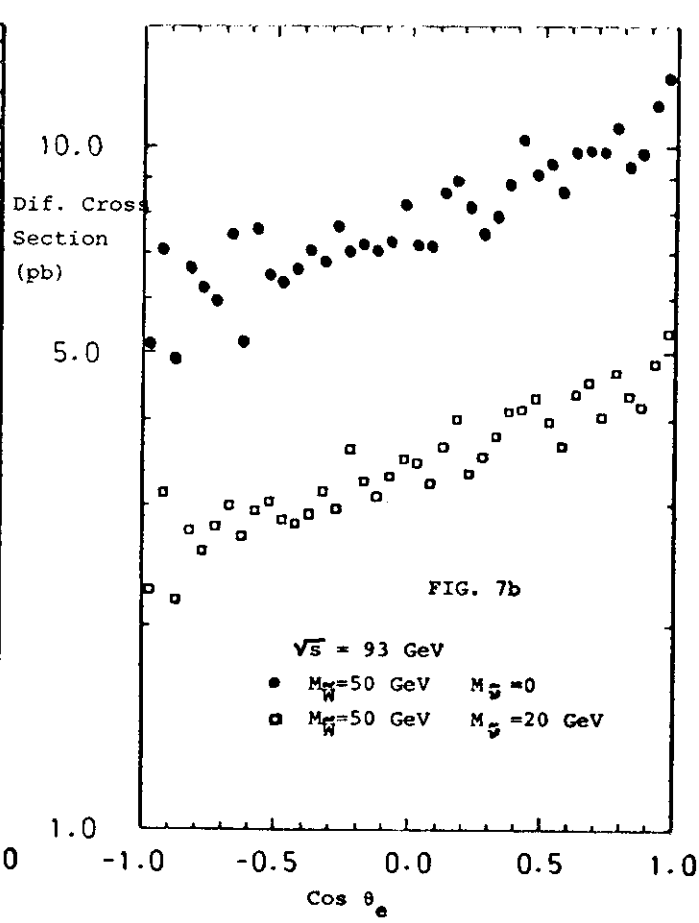
10.0
Dif. Cross
Section
(pb)
5.0
1.0
FIG. 7b
√s = 93 GeV
● $M_{\tilde{W}}$=50 GeV $M_{\tilde{\nu}}$=0
□ $M_{\tilde{W}}$=50 GeV $M_{\tilde{\nu}}$=20 GeV
-1.0
-0.5
0.0
0.5
1.0
Cos θ_e

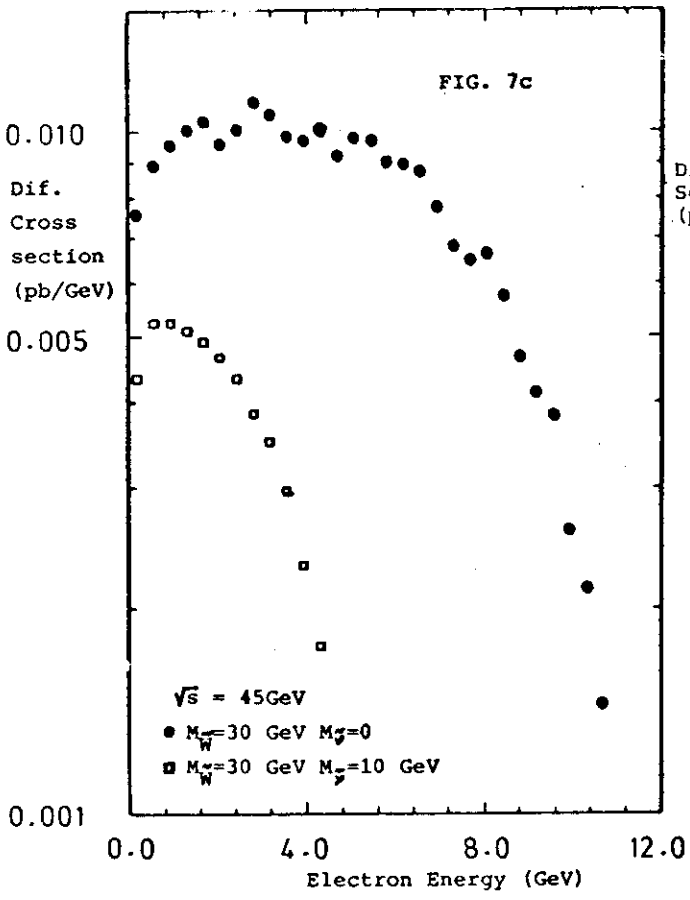
FIG. 7c
0.010
Dif.
Cross
section
(pb/GeV)
0.005
0.001
$\sqrt{s}$ = 45GeV
● $M_{\tilde{W}}$=30 GeV $M_{\tilde{\gamma}}$=0
□ $M_{\tilde{W}}$=30 GeV $M_{\tilde{\gamma}}$=10 GeV
0.0
4.0
8.0
12.0
Electron Energy (GeV)

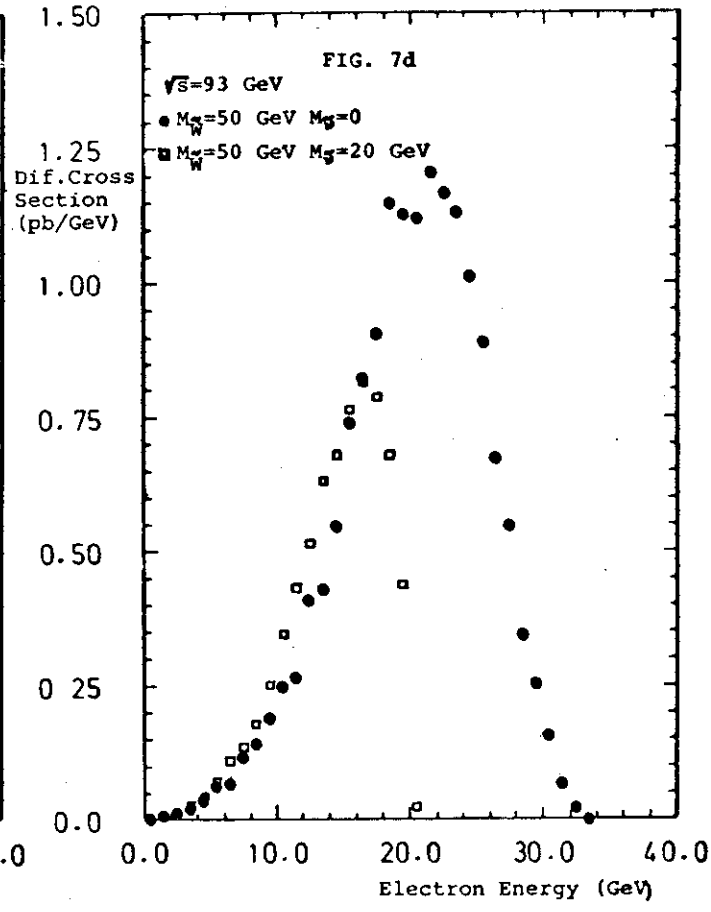
FIG. 7d
$\sqrt{s}$=93 GeV
● $M_{\tilde{W}}$=50 GeV $M_{\tilde{\gamma}}$=0
□ $M_{\tilde{W}}$=50 GeV $M_{\tilde{\gamma}}$=20 GeV
1.50
1.25
Dif.Cross
Section
(pb/GeV)
1.00
0.75
0.50
0 25
0.0
0.0
10.0
20.0
30.0
40.0
Electron Energy (GeV)